Hindawi Publishing Corporation
International Journal of Rotating Machinery
Volume 2016, Article ID 5834172, 8 pages
http://dx.doi.org/10.1155/2016/5834172

Research Article

Effect of the Modification of the Start-Up Sequence on the Thermal Stresses for a Microgas Turbine

Oscar Tenango-Pirin,[1] J. C. García,[1] Laura Castro-Gómez,[1] J. A. Rodríguez,[1] F. Sierra,[1] Oscar De Santiago,[2] and J. M. Rodríguez-Lelis[3]

[1]*Universidad Autónoma del Estado de Morelos (UAEM), Universidad 1001, Colonia Chamilpa, 62209 Cuernavaca, MOR, Mexico*
[2]*ETU i+D, Cuauhtémoc 3, Colonia Industrial San Pedrito Peñuelas, 76148 Querétaro, QRO, Mexico*
[3]*Centro Nacional de Desarrollo Tecnológico, Interior Internado Palmira s/n, Colonia Palmira, 62490 Cuernavaca, MOR, Mexico*

Correspondence should be addressed to J. C. García; jcgarcia@uaem.mx

Received 31 December 2015; Accepted 17 April 2016

Academic Editor: Jiun-Jih Miau

Microgas turbines (MGT) are an alternative for small-scale energy production; however, their small size becomes a drawback since it enhances the heat transfer among their components. Moreover, heat transfer drives to temperature gradients which become higher during transient cycles like start-up. The influence of different start-up curves on temperature and thermal stresses of a microgas turbine was investigated. Stationary and rotational blades of the turbine were numerically simulated using CFD and FEM commercial codes. Conjugated heat transfer cases were solved for obtaining heat transfer from fluid toward the blades. Changes of temperature gradients within the blades during the start-ups were calculated under transient state with boundary conditions according to each curve to assess accurate thermal stresses calculations. Results showed that the modification of the start-up curves had an impact on the thermal stresses levels and on the time when highest stresses appeared on each component. Furthermore, zones highly stressed were located near the constraints of blades where thermal strains are restricted. It was also found that the curve that had a warming period at the beginning of the start-up allowed reducing the peaks of stresses making it more feasible and safer for the turbine start-up operation.

1. Introduction

It is well known that thermal stresses in materials are caused by temperature gradients and mechanical constraints. Turbomachinery is often subjected to that condition, with the gas turbines being the most affected due to they work with high temperature gases [1, 2]. This is because for higher turbine inlet temperatures the efficiency of the turbine is improved; however, the turbine components life in creep is reduced. In addition, when a turbine is employed for power generation, continuous operation is required; hence thermal and structural analyses of its components for a reliable operation become necessary.

In a turbine, fixed and rotational blades are the components that have interaction with inlet gases when they are at the highest temperature. Moreover, as a result of energy transformation, temperature and pressure of fluid change giving rise to nonuniform temperature distributions. This condition, together with the constraints on the bases of each component, drives to thermal stresses development. That problem becomes stronger in microgas turbines because their small size makes it complicated to employ cooling methods like internal cooling holes, which enhances the heat transfer among the components and limits the material strain.

When a turbine is subjected to start-up and shutdown cycles, thermal stresses reach their highest values owing to heating and cooling periods. During these cycles, highest temperature gradients and thermal stresses are developed in short periods of time, which could lead to thermal fatigue through Low Cycle Fatigue (LCF). Some studies have been carried out in order to investigate parameters that have influence on thermal stresses development during start-up cycles. Nowak and Rusin investigated the influence of several start-up velocities on the lifetime of a steam turbine rotor

[3]. They found that thermal stresses states and the durability of turbine components are modified by start-up velocities. On the other hand, stress levels in a steam drum of a heat recovery steam generator were reduced by Kim et al. through the modification of the start-up curve [4]. Also, thermal stresses of the high pressure rotor (HPR) of a turbine were reduced by initially heating the rotor while it rotates at the minimum possible frequency [5], being the initial temperature of the material another key parameter for stress behavior. Meanwhile, other studies [6, 7] concluded that selecting the appropriate material for turbine manufacturing has an influence on thermal elongation because of material properties. Nevertheless, most of the studies of start-ups are focused on components (mainly rotors) of industrial turbines and there is lack of analyses addressed to microgas turbines.

In a previous work, thermal stresses curves and temperature fields in an axial microgas turbine were calculated during design phase by performing the linear start-up simulation until nominal speed was reached [8]. However, peaks of high stress levels nearly the material yield strength were obtained. In this work, the influence of different start-up curves on the thermal stress levels is investigated by applying Computational Fluid Dynamics (CFD) and Finite Element Method (FEM) analyses. The aim of the study is to look for the decrease in stress levels by modifying start-up curves and velocities like some of the works aforementioned. In this way, information for a reliable and less damaging start-up of the MGT is provided.

2. Materials and Methods

2.1. Geometry of the Model. The model of the axial turbine under study is presented in Figure 1. The turbine is a one-stage impulse type and it is constituted by 17 static blades (hereafter referred as nozzle) and 32 rotating blades. It was designed to supply a shaft power of around 29 kW and to work under simple Brayton Cycle [9]. For the analysis of the blades, transient conjugated heat transfer (CHT) and static structural analyses were conducted by using CFD and FEA; Fluent and Ansys were implemented, respectively. First, fluid dynamic of hot gases was solved to figure out the temperature distributions on the components; afterwards, temperature results were used as boundary condition for thermal stresses calculation.

2.2. Start-Up Curves. Simulations of three different start-up curves labeled as numbers 1, 2, and 3 in Figure 2 were done. Start-up 1, where a linear curve was assumed, was previously simulated in [8] and it was taken as reference. Start-ups curves range from cold start until rated speed of the turbine is reached at 240 s. The proposed curves 2 and 3 have an exponential and logarithmic behavior, respectively, making mass flow increment more intense in some periods and softer in other ones. Calculations were carried out in each temporal point indicated in the curves of Figure 2. It should be noted that the number of points was increased in some regions for a better resolution of the higher stresses. Meanwhile, mass flow of gases and rotational velocity were increased by steps; therefore, in each temporal point calculations of temperature

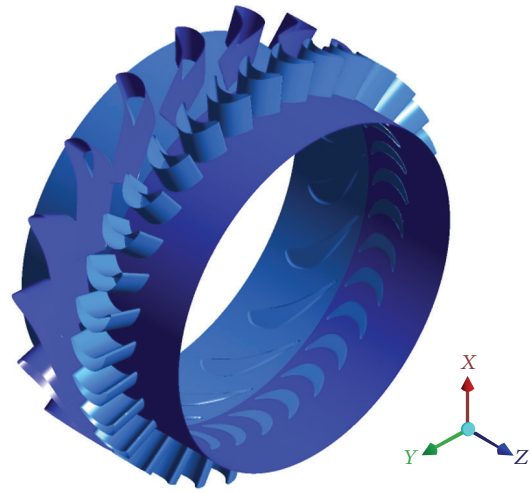

Figure 1: Three-dimensional geometry of the expansion turbine.

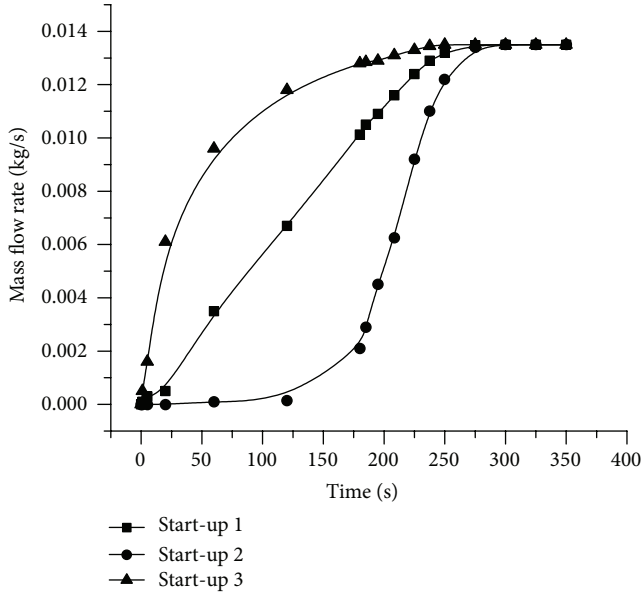

Figure 2: Turbine start-up curves simulated.

distribution and thermal stresses were carried out. At full operating speed, turbine rotation reaches 76 000 rpm and mass flow is 0.0135 kg/s. Time steps were varied from 0.001 to 10 s along each curve for transient calculations.

2.3. Numerical Methodology

2.3.1. Computational Grid. The discretization of the control volumes was done using ICEM-CFD program for both the flow domain and the solid domain. A mesh convergence analysis was conducted employing the equations proposed by Roache [10]. Four nonstructured meshes of different number of tetrahedral elements were used. After the analysis, a mesh conformed by 786,088 elements was selected to perform the calculations. The mesh is presented in Figure 3 where the

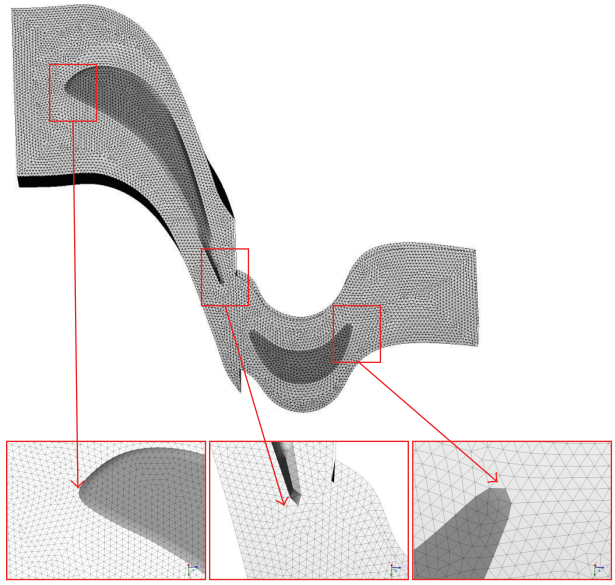

Figure 3: Passage mesh and zoom up of grids employed.

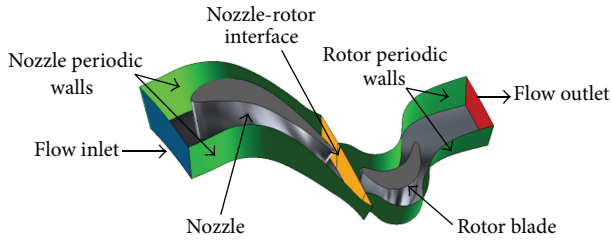

Figure 4: Flow channel geometry and boundary conditions.

type of element is emphasized. Due to the geometry which is axially symmetric, only one turbine passage that includes one static blade passage and one rotating blade passage was modeled, Figure 4.

2.3.2. Boundary Conditions. The numerical domain and the boundary conditions used for the CFD computation are shown in the model of Figure 4. In order to ensure fluid continuity through the domain and to obtain a single passage, an interface between nozzle and rotor was generated. In the lateral walls of the passage, rotational periodicity conditions were assigned. At solid boundaries, the no-slip condition was used and the thermal conductivity of the material was also utilized for a coupled heat transfer prediction including both conduction and convection mechanisms. At inlet and outlet, mass flow and pressure conditions were considered, respectively. The working fluid coming from the combustion chamber was considered as compressible and its temperature was kept constant but mass flow rate at turbine inlet was varied based on each curve of Figure 2 having an influence on both the temperature distribution and the heat exchange between fluid and blades.

Finite Element Method has been recognized by its capability to calculate thermal stresses and deformations allowing

Table 1: Mechanical properties of the alloy.

Physical properties of Nimonic 105	
Young's modulus (E)	154 GPa
Density (ρ)	8010 kg/m^3
Specific heat (Cp)	586 J/kg°C
Poisson's ratio (ν)	0.3
Thermal expansion coefficient (α)	14.0×10^{-6}/°C
Thermal conductivity (k)	18.63 W/m°C

determining and predicting failures in turbomachinery [11, 12] and it is often used as a design tool. FEM was implemented for solving the structure analysis of materials. The same mesh generated for the CFD analysis was employed, excluding the fluid domain in order to have only the solid domain. Temperature data obtained from CFD calculations was assigned as thermal load through using an external algorithm. Bases of both nozzle and blade were restricted to any elongation to resemble the join to the turbine casing and rotor, respectively. The mechanical properties were assigned corresponding to Nimonic 105 alloy [13], which has the properties at room temperature presented in Table 1. The material is used for gas turbine blades manufacturing, its yield strength is 853 MPa, and it was created to operate beyond 1225 K. The material was considered neglecting any cooling method or thermal barrier coating (TBC).

2.3.3. Governing Equations. In this section main equations and models for the calculations are summarized. Flow dynamics through the turbine was firstly predicted by solving the continuity, momentum, and energy equations considering the flow as compressible, transient, three-dimensional, and turbulent. The 3D Reynolds Averaged Navier Stokes (RANS) equations were employed and Reynolds stresses were modeled with Boussinesq hypothesis. For turbulence modeling the Spalart-Allmaras model was chosen based on the good results provided for numerical studies of blade turbines [14]. It is a one equation model which models the transport equations with a modified form of the turbulent kinematic viscosity called kinematic eddy viscosity $\tilde{\nu}$:

$$\begin{aligned}\frac{\partial}{\partial t}\left(\rho\tilde{\nu}\right) + \frac{\partial}{\partial x_i}\left(\rho\tilde{\nu}u_i\right) &= G_\nu + \frac{1}{\sigma_{\tilde{\nu}}}\left[\frac{\partial}{\partial x_i}\left\{\left(\mu + \rho\tilde{\nu}\right)\frac{\partial\tilde{\nu}}{\partial x_j}\right\} + C_{b2}\rho\left(\frac{\partial\tilde{\nu}}{\partial x_j}\right)^2\right] \\ &\quad - Y_\nu + S_{\tilde{\nu}},\end{aligned} \tag{1}$$

where Y_ν is the destruction of turbulent viscosity occurring in the near-wall region and G_ν is the production of turbulent viscosity whose definition can be found in [15]. Furthermore, it has been extended in Fluent software giving the advantage of using wall functions for meshes that are not fine enough.

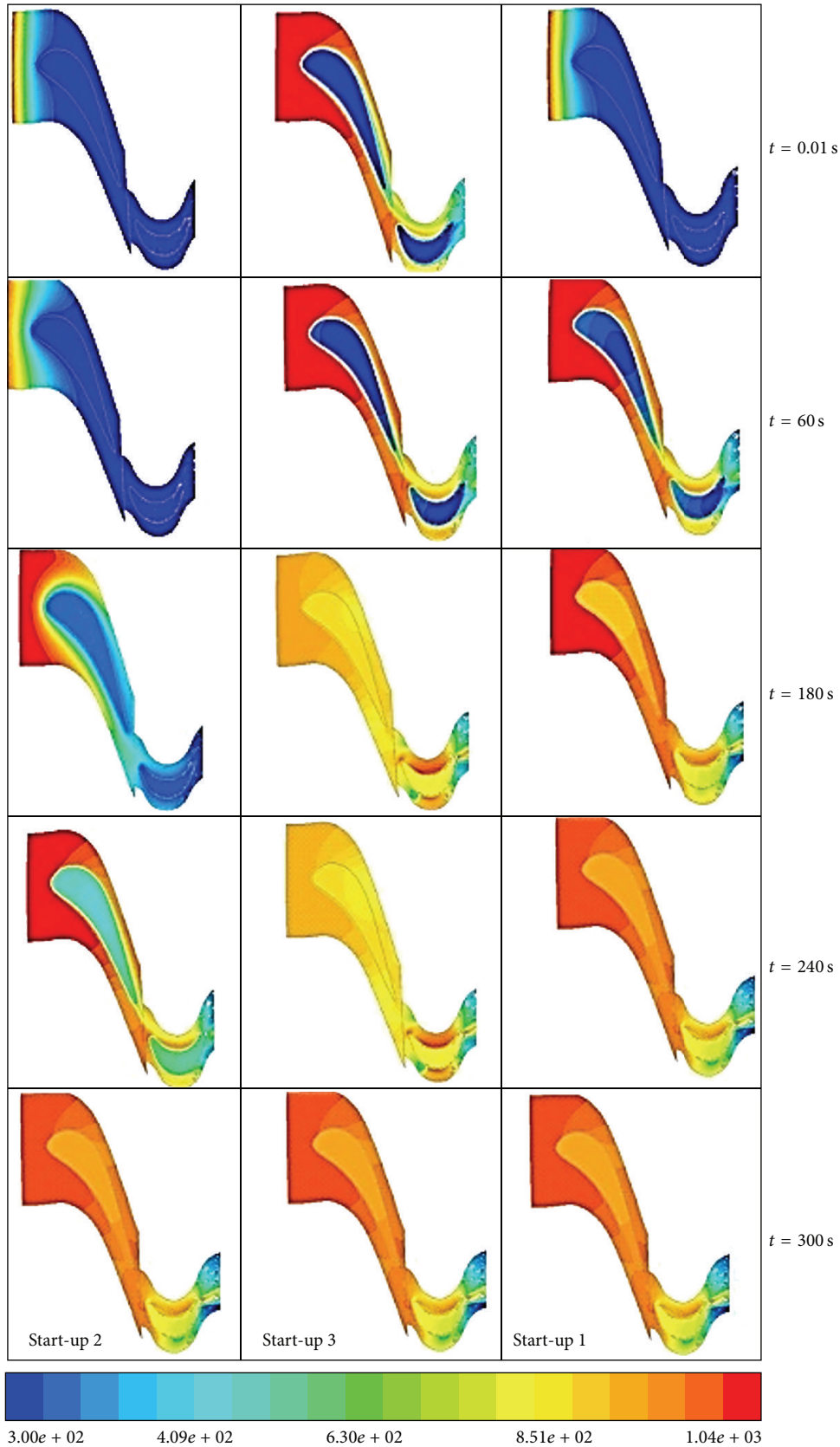

Figure 5: Temperature contours in K obtained in each start-up.

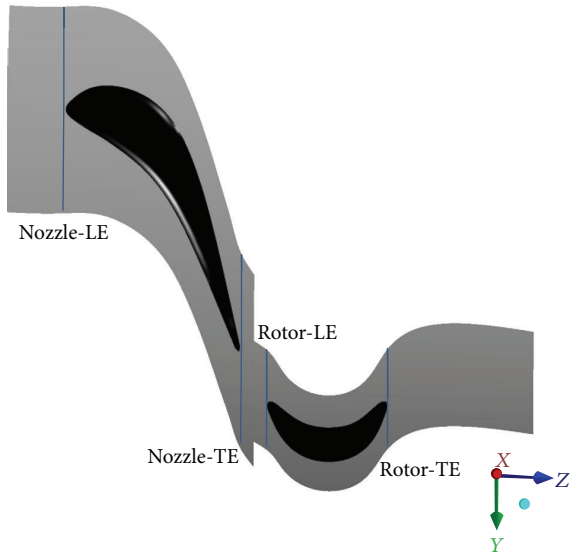

Figure 6: Profiles where temperatures were extracted.

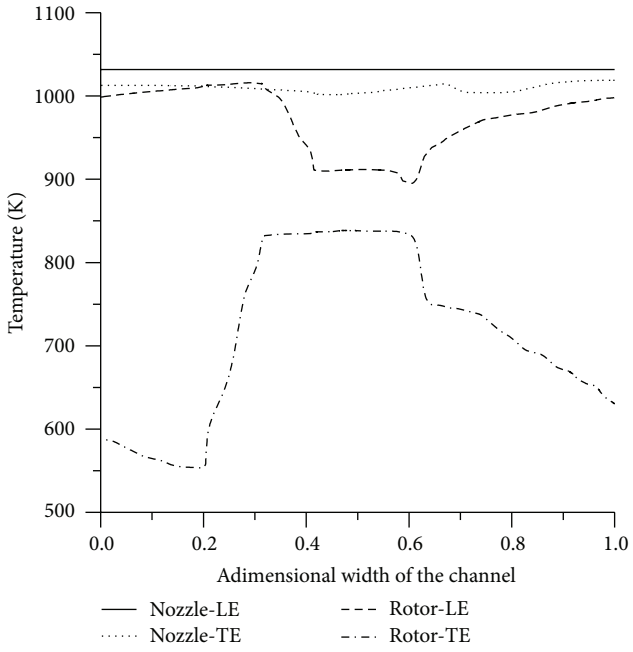

Figure 7: Temperature distributions obtained from the profiles.

In this study, a coarse mesh was used in the near-wall region; hence, law of the wall was employed:

$$\frac{u}{u_\tau} = \frac{1}{k} \ln E \left(\frac{\rho u_\tau y}{\mu} \right), \tag{2}$$

where u is the velocity parallel to the wall, u_τ is the shear velocity, k is the Von Kármán constant, and $E = 9.793$. The rotation of the turbine was taken into account by implementing the Sliding Mesh model. This model allowed varying the rotational velocity of the blade which was increased according to the mass flow rates shown in Figure 2. Meanwhile, properties of the flow as density, specific heat, and viscosity were defined as ideal gas and constants for each temporal step. SIMPLE algorithm was used for pressure-velocity coupling.

On the other hand, thermal stresses were calculated using the material properties like elastic modulus (E) and coefficient of thermal expansion (α) and temperature gradients (ΔT): $\sigma = E\alpha\Delta T$. Equivalent stresses were taken to analyze the results by the representation of Von-Mises stresses:

$$\sigma_{\text{eff}} = \left[\frac{(\sigma_1 - \sigma_2)^2 + (\sigma_2 - \sigma_3)^2 + (\sigma_3 - \sigma_1)^2}{2} \right]^{1/2}. \tag{3}$$

3. Results and Discussion

3.1. Analysis of Temperature Distribution. Even though calculations were done throughout all start-up curves, results where highest temperature and stress levels appeared were selected in order to make a more detailed analysis. Figure 5 illustrates the temperature contours in a midplane along the axial direction of turbine passage for some temporal points. It can be seen that stationary thermal state is reached at 300 seconds for all the curves. Both start-up curves 2 and 3 showed a more intense components heating in short periods of time, while curve 1 heating was constant and linear throughout the start-up. In comparison with start-up 1, most heating of components during start-up 2 occurred after 180 seconds at the end of the curve. In contrast, start-up 3 shows a faster components heating during the first time steps, such that, at 180 seconds, stationary state and highest temperatures were almost reached. This is a consequence of a higher mass flow increment in short lapses as Figure 2 shows, leading to the most heat transfer toward the turbine components during those periods. Highest temperature values of 1005 K and 935 K were located at nozzle trailing edge and blade leading edge, respectively, and they are near the gas temperature. Coldest zones were at nozzle center and blade trailing edge. As a result, temperature distribution within the components was not uniform and it varies in the axial, tangential, and radial directions causing the temperature gradients development.

Temperature distribution obtained from the profiles marked on the plane of Figure 6, when stationary state has been reached, is shown in Figure 7. In the nozzle, temperature levels along Nozzle-LE and Nozzle-TE profiles are almost the same, because even though fluid expansion occurs, static temperature drop does not occur. On the other hand, temperature differences between Rotor-LE and Rotor-TE profiles are noticeable. That is a consequence of thermal energy conversion into mechanical energy on the blades. Meanwhile, temperature distributions in the suction side are smaller than those on the pressure side where energy conversion takes place.

3.2. Thermal Stresses Analysis. In this section, thermal stresses through the representation of Von-Mises stresses are analyzed. Highest values of stresses obtained in each component along the curves were obtained and they are shown in Figure 8. The values were taken from each temporal point allowing identifying the time when maximum values

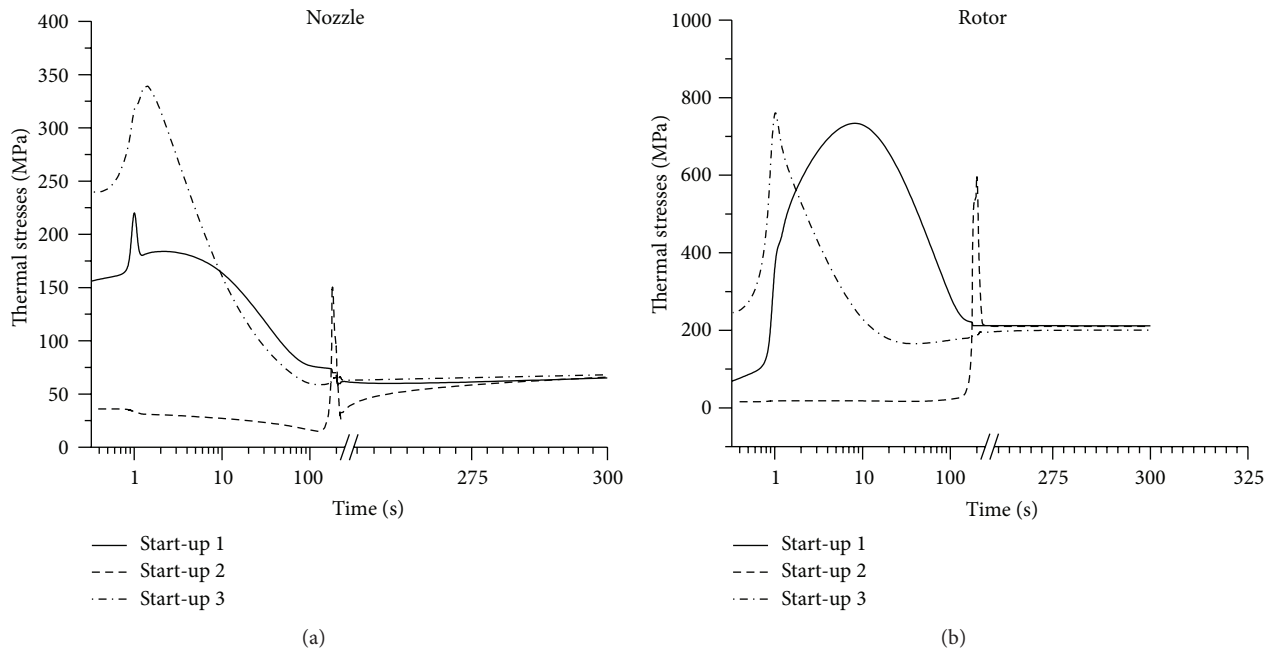

Figure 8: Highest thermal stresses variation on the components during start-ups.

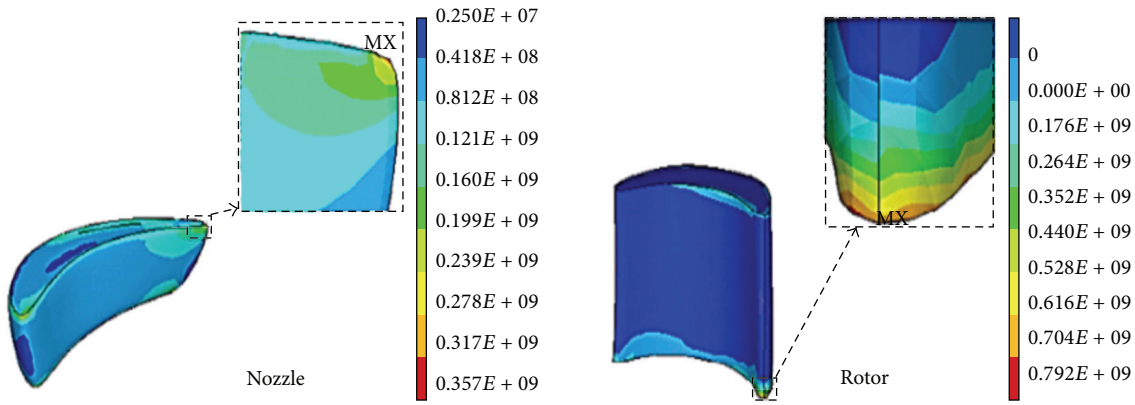

Figure 9: Von-Mises stresses contours on the components, units in Pa.

of Von-Mises stress appeared. Only one significant stress amplitude (peak) in each curve can be seen. On the blade, stress level in start-up 3 was practically the same like start-up 1 having a marginal difference about 1 MPa. Highest stress peak in the turbine appeared in the blade leading edge during start-up 3 with a value of 793 MPa. Meanwhile, the lowest stress peaks were developed in start-up 2 having values of 150 and 596 MPa for the nozzle and blade, respectively. It can also be noticed from Figure 8 that times when highest stress peaks appear in start-up 2 are separated from the two remainders, due to the highest gas mass flow at the end of the curve.

Contours of highest Von-Mises stresses in each component are illustrated in Figure 9. On the nozzle, highest thermal stress of 356 MPa was developed during start-up 3; it was located at the trailing edge at the near casing region where the nozzle is fixed. From the thermal analysis results, highest temperature was obtained in the same zone and it produced the temperature gradient giving rise to the stress. Moreover, it can be seen that high stress values were concentrated at the leading edge and stress in the pressure side was higher than on the suction side. On the other hand, highest stress levels corresponding to the blade were obtained during start-up 3 as well. A value of 793 MPa was reached appearing in the leading edge as illustrated in Figure 9 having a coincidence with the place with highest temperature. In addition, contours revealed stressed zones along the blade base and in a portion of the tip.

The monitoring locations with highest stress levels, shown in Figure 10, were selected as critical points for getting their temporal evolution during the start-ups. Critical points are labeled as NTET and RLEB for the nozzle and rotor, respectively. Stress curves obtained from NTET point are shown in Figure 11. In start-up curves 1 and 3, highest peaks were developed at the simulated time of 1 second, while in

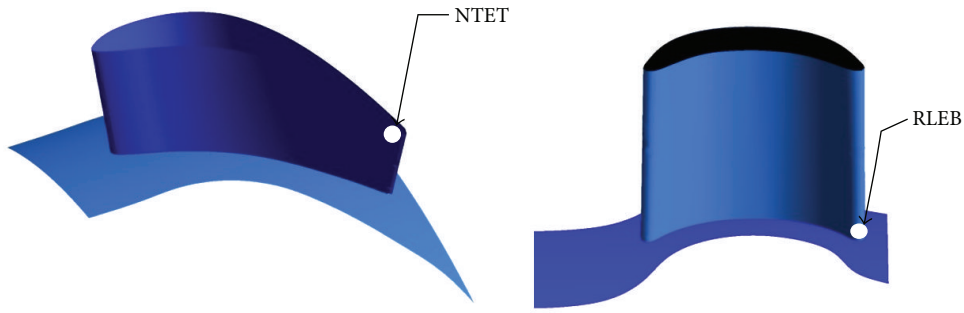

Figure 10: Critical points where thermal stresses were analyzed.

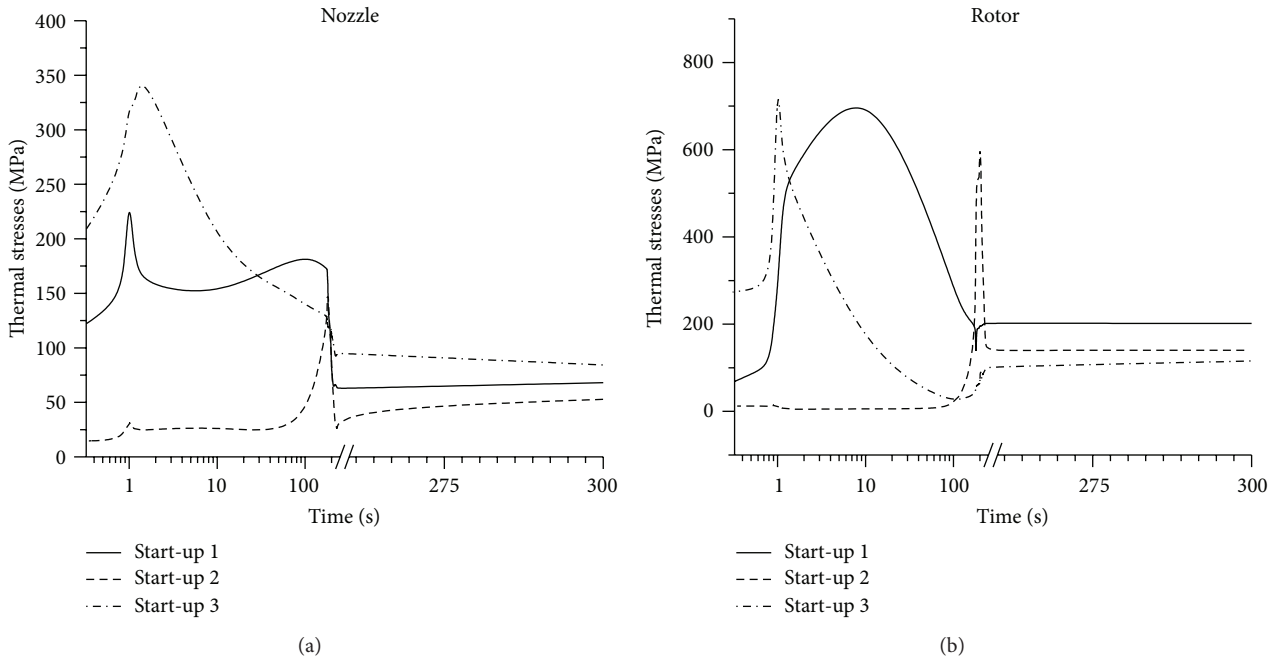

Figure 11: Stress evolution in the critical zones.

start-up 2 the highest peak was presented at 180 seconds. Lowest peak was located in start-up 2 being equivalent to 150 MPa. Stress oscillation can also be seen in start-up curves 1 and 3. Those oscillations suggest repetitive elongation and compression deformations of the material which are not desirable due to the fact that they could contribute to the LCF. In addition, stress record of blade is also presented in Figure 11. Levels of peak of start-ups curves 1 and 3 were similar but they were presented at different times, while the one of curve 2 was the lowest at 200 seconds. Lowest peak was equivalent to 596 MPa being significantly below the highest peak. This is attributed to material warming at the beginning of the curve minimizing the temperature gradients near the nominal speed of turbine.

Positive stress levels values were generated in all curves suggesting deformations of the material without returning to its original shape at any time. This in turn induces thermal damages which are accumulated and reduce the remaining life of the material according to Miner's rule [16]. That is the reason why they should be reduced. Moreover, start-up curve 2 in each component showed a noticeable deviation of the reference curve, stress levels, for instance. Nevertheless, due to high stress levels reached, further analyses of fatigue and creep on the material are advisable; however, they are beyond the objectives of this work.

4. Conclusions

This paper illustrates both thermal and structural analyses by employing the simulation of three different start-up curves of MGT. Results showed that velocity of rotation and mass flow rate had an influence on heating of the components which varied for each curve. Consequently, that had an influence on thermal stress behavior and levels. It was shown that despite any start-up curve modification, zones of the components where highest thermal stresses and temperatures are obtained were not affected; however, times and levels were varied. As regards levels of stress, they were under yield strength of material and some oscillations in stress evolution were obtained for curves 1 and 3 as a consequence of the

deformations of the material. On the other hand, start-up curve 2 was selected as the more viable curve for the turbine operation because of the lowest peaks of stresses and no development of oscillations in stress evolution was observed. With that curve, highest thermal stress levels values were reduced about 25%, which benefits for the service life of the turbine.

Competing Interests

The authors declare that they have no competing interests.

Acknowledgments

The authors would like to acknowledge to the CONACYT 206393 project for the financial support.

References

[1] Y. Xie, K. Lu, L. Liu, and G. Xie, "Fluid-thermal-structural coupled analysis of a radial inflow micro gas turbine using computational fluid dynamics and computational solid mechanics," *Mathematical Problems in Engineering*, vol. 2014, Article ID 640560, 10 pages, 2014.

[2] S. Guo, "Investigations on the blade vibration of a radial inflow micro gas turbine wheel," *International Journal of Rotating Machinery*, vol. 2007, Article ID 29270, 10 pages, 2007.

[3] G. Nowak and A. Rusin, "Lifetime deterioration of turbine components during start-ups," *Operation Maintenance and Materials Issues*, vol. 3, no. 1, pp. 1–10, 2004.

[4] T. S. Kim, D. K. Lee, and S. T. Ro, "Analysis of thermal stress evolution in the steam drum during start-up of a heat recovery steam generator," *Applied Thermal Engineering*, vol. 20, no. 11, pp. 977–992, 2000.

[5] A. A. Ivanovskii, V. L. Pokhoriler, and V. N. Goloshumova, "Calculating the thermally stressed state of the high and medium pressure rotors of a T-250/300-240 turbine in the labyrinth seal zone," *Power Technology and Engineering*, vol. 42, no. 2, pp. 100–104, 2008.

[6] W. Kosman, M. Roskosz, and K. Nawrat, "Thermal elongations in steam turbines with welded rotors made of advanced materials at supercritical steam parameters," *Applied Thermal Engineering*, vol. 29, no. 16, pp. 3386–3393, 2009.

[7] A. H. Mustafa, M. S. Hashmi, B. S. Yilbas, and M. Sunar, "Investigation into thermal stresses in gas turbine transition-piece: influence of material properties on stress levels," *Journal of Materials Processing Technology*, vol. 201, no. 1–3, pp. 369–373, 2008.

[8] T. P. Oscar, J. C. García, F. Z. Sierra et al., "Numerical calculation of thermal stresses in a micro gas turbine," in *Memorias del XIX Congreso Internacional Anual de la SOMIM*, Pachuca, Mexico, September 2013.

[9] A. Alonzo, J. C. García, F. Sierra, and A. Rodríguez, "Cálculo de Flujo en un a Microturbina de Gas Usando Dinámica de Fluidos Computacional," in *Memorias del XII Conferencia Latinoamericana de Turbomaquinaria*, Querétaro, México, March 2012.

[10] P. J. Roache, *Fundamentals of Computational Fluid Dynamics*, Hermosa, Albuquerque, Nuevo Mexico, 1998.

[11] M. R. Kohle, A. D. Pachchhao, and H. G. Nagpure, "Thermal stress analysis in steam turbine rotor—a review," *IOSR Journal of Mechanical and Civil Engineering*, pp. 83–86, 2014.

[12] L. Witek, M. Orkisz, P. Wygonik, D. N. Musili, and T. Kowalski, "Fracture analysis of a turbine casing," *Engineering Failure Analysis*, vol. 18, no. 3, pp. 914–923, 2011.

[13] Special Metals Corporation, *NIMONIC® Alloy 105*, Publication SMC-081, Special Metals Corporation, New Hartford, NY, USA, 2007, http://specialmetals.com/documents/Nimonic%20alloy%20105.pdf.

[14] H. R. Alejandro, M. C. Zdzislaw, D. Alain, and J. A. López Hernandez, "The effect of start-up cycle in ceramic coating used as thermal barrier for a gas turbine bucket," *Applied Thermal Engineering*, vol. 29, no. 14-15, pp. 3056–3065, 2009.

[15] Ansys Inc, *Ansys Fluent 14.1 Theory Guide*, Ansys Inc, 2011.

[16] J. Schijve, "Fatigue of structures and materials in the 20th century and the state of the art," *International Journal of Fatigue*, vol. 25, no. 8, pp. 679–702, 2003.